Slow, heterogeneous NFκB single molecule conformational dynamics and implications for function

Wei Chen[1], Wei Lu[2], Peter G. Wolynes[2] and Elizabeth A. Komives[1,*]

[1]Department of Chemistry and Biochemistry, University of California, San Diego, 9500 Gilman Drive, La Jolla, CA 92093-0378.

[2] Center for Theoretical Biological Physics, Departments of Chemistry, Physics, and Biosciences, Rice University, Houston, Texas, United States of America.

*Elizabeth A. Komives

Email: *ekomives@ucsd.edu

Abstract

The transcription factor NFκB (RelA-p50) is a multidomain protein that binds DNA and its inhibitor, IκBα with apparently different conformations. We used single-molecule FRET to characterize the interdomain motions of the N-terminal DNA-binding domains in the free protein and also in various bound states. Several surprising results emerged from this study. First, the domains moved with respect to each other on several widely different timescales from hundreds of milliseconds to minutes. The free NFκB displayed stochastic motions leading to a broad distribution of states, ranging from very low-FRET states to high-FRET states. Varying the ionic strength altered the slow motions suggesting that they may be due to different weak electrostatic interactions between the domains creating a rugged energy landscape. Third, the DNA-binding domains continued to be mobile even when the protein was bound to its cognate DNA, but in this case the majority of the states were either high-FRET, a state expected from the available x-ray structures, or low-FRET, a state consistent with one of the DNA-binding domains dissociated. The fluctuations of the DNA-bound states were of lower amplitude and slightly slower rate. Fourth, the inhibitor, IκBα freezes the domains into a low-FRET state, expected to be incapable of binding DNA. Neutralization of five acidic residues in the IκBα PEST sequence, which was previously shown to impair IκBα's ability to strip NFκB from the DNA, also impaired its ability to freeze the domains into a low-FRET state indicating that the freezing of motions of the DNA-binding domains is essential for efficient molecular stripping.

Significance Statement

The relative domain motions of multidomain proteins regulate many aspects of cellular functions. However, experimental characterization of such motions has been challenging. Here, we use single-molecule FRET to resolve the domain motions of the transcription factor NFκB. Our results reveal slow and heterogeneous motions on a broad range of timescales from hundreds of milliseconds to minutes, which are altered by DNA binding and completely locked by the inhibitory protein, IκBα. Our results suggest that such slow motions originate from electrostatic interactions and are essential in regulating the kinetics of DNA association and dissociation.

Introduction

Functional coordination of different domains is crucial for multidomain proteins, which comprise over two thirds of the eukaryotic proteome (1). The relative orientations and motions of the domains are important for macromolecular recognition, especially for efficient and reversible interactions required in cellular signaling (2). However, the interdomain dynamics cannot be understood with static pictures or studies on individual domains. It remains largely unknown how the domains are oriented with respect to one another in protein assemblies, how they re-orient during macromolecular interactions and how the interdomain dynamics affects molecular recognition.

Here we focus on the multidomain transcription factor NFκB RelA-p50 heterodimer (hereafter referred to as NFκB). Dimerization among members of the same protein family is prevalent for eukaryotic transcription factors (3). Theoretical studies suggest that the relative motions of the two DNA-binding domains in a transcription factor dimer control the search and recognition of target DNA (4). The NFκB monomer consists of a dimerization domain (DD) and a N-terminal DNA-binding domain (NTD) connected by a 10-amino acid linker. The NFκB dimer recognizes the consensus κB DNA sequence with its two NTDs (Fig. 1*A*). No crystal structures are available for NFκB in the absence of binding partners. We previously showed using molecular dynamics (MD) simulations corroborated by hydrogen-deuterium exchange experiments that the flexible linkers allow the two NTDs to undergo large-scale relative domain motions which leads to exposure of the DNA-binding cavity in RelA-p50 (5).

NFκB responds to a large number of extracellular stimuli and activates hundreds of genes. In the absence of stimuli, NFκB is held inactive in the cytoplasm by the inhibitor protein, IκBα. Upon stimulation, the IκB kinase is activated to phosphorylate NFκB-bound IκBα, which is then ubiquitylated and degraded by the proteasome (Fig. 1*C*) (6). Degradation of IκBα exposes the NFκB nuclear localization signal and shifts the intracellular distribution of NFκB from the cytoplasm to the nucleus. There are over 10^4 NFκB binding sites in the human genome, primarily in promoter and enhancer regions (7). NFκB also activates the expression of its own inhibitor, IκBα, creating a negative feedback loop in which the newly synthesized IκBα enters the nucleus, binds to NFκB to block DNA binding (8), and return the NFκB-IκBα complex to the cytoplasm (9). In the crystal structures of IκBα-bound NFκB, the NTD of p50 is truncated in order to achieve crystallization (Fig. 1*B*) (10, 11), and therefore the relative orientation of the NTDs in NFκB-IκBα is unknown

As a master regulator of hundreds of genes, the termination of NFκB signaling must be efficient. Previous kinetic experiments revealed molecular stripping—a process in which IκBα actively removes NFκB from DNA (6). This discovery suggests that the termination of NFκB signaling is not just an equilibrium result of IκB outcompeting DNA for binding to NFκB but rather it is achieved kinetically through IκBα-accelerated dissociation of NFκB from DNA. A transient ternary complex was observed during molecular stripping, and the DNA dissociation rate is proportional to the IκBα concentration (12). A stripping impaired IκBα mutant generated by neutralizing the negatively PEST sequence results in slower nuclear export of NFκB in the cell (13). Coarse-grained MD simulations suggest that conformational dynamics of the NFκB NTDs and the disordered PEST sequence of IκBα play key roles in the mechanism of molecular stripping (14, 15). In the simulations, IκBα appeared to twist the relative orientation of the two NTDs in the NFκB dimer to a conformation where only one of the NTDs can bind DNA. The simulations predicted that the conformational change in the NTDs would weaken the NFκB-DNA interaction and therefore lower the dissociation barrier. In addition, the negatively charged PEST sequence of IκBα appeared to displace DNA in the binding pocket and electrostatically repel DNA so as to prevent DNA rebinding (15).

Here we report the relative domain motions of the NFκB NTDs in the free, DNA-bound, and IκBα-bound states revealed by single-molecule FRET (smFRET). The NTDs moved with respect to each other on different timescales ranging from hundreds of milliseconds to minutes, revealing a hierarchical rugged energy landscape. The free NFκB displayed stochastic interdomain motions dependent on ionic strength generating a broad distribution of conformations

with inter-NTD distances from 30 Å to 70 Å. The NTDs remained mobile even when bound to DNA, but in this case the conformational ensemble was shifted so as to display two major populations—a high-FRET state expected from NFκB-DNA crystal structures (16) and a low-FRET state consistent with only one of the NTDs bound to DNA. Binding of the inhibitor protein, IκBα, appears to completely lock the NFκB NTDs into a single conformation consistent with NTDs being spread apart. We finally show that the PEST sequence is required for this locking function because NFκB bound to the stripping-impaired IκBα 5xPEST mutant retains its broad ensemble of structures and their interconversion. The smFRET detected by total internal reflection fluorescence (TIRF) microscopy reveals slow and heterogeneous domain motions in NFκB that are modulated in different ways by DNA- or IκBα binding. We speculate that despite the fact that such slow motions have not, to our knowledge, been reported in other protein systems, they are essential for efficient molecular stripping and readily account for the intracellular kinetics observed for NFκB.

Results

Conformational Heterogeneity in Free NFκB. Previous coarse-grained (14) and all-atom MD simulations (5) showed that the two NTDs in a NFκB dimer can rotate and translate with respect to each other. To experimentally probe the conformational heterogeneity of the NTDs, we carried out TIRF-based smFRET experiments by labeling each NTD with either a donor or acceptor fluorophore. We replaced RelA Glu128 and p50 Phe148 with p-azidophenylalanine (pAzF) by amber suppression and then labeled these two residues specifically with either Alexa Fluor 555 or Alexa Fluor 647 sDIBO alkyne via click chemistry (17, 18). The distances between the labeling positions in the NFκB-DNA crystal structure (16) and in an open conformation obtained from previous all-atom simulations (5) are 27 Å and 70 Å respectively, which correspond to 0.1 and 1 in FRET efficiency given the dye pair R_0 of 51 Å (Fig. 2*A*). The dual-labeled NFκB was immobilized on the DT20 passivated slide (19) through a series of interactions between the C-terminal His-tag on RelA, biotin anti-His antibody, NeutrAvidin, and biotin-bovine serum albumin (BSA) (Fig. 2*B*). We collected 426 smFRET traces for free NFκB (Fig. S6-32). Each smFRET trace covers between 10 and 300 seconds depending on the photobleaching lifetime of the fluorophores. The experimental FRET histogram, calculated from the first 10 seconds to avoid bias caused by long traces, showed a broad distribution in FRET efficiency from 0.1 to 1 (Fig. 2*C*), revealing a conformational heterogeneity which corresponds to approximate distances of 30 Å - 70 Å. The distances we report are close estimates based on rigorous background and donor leakage corrections. Obtaining accurate distances from smFRET requires alternating two-color laser excitation (20) and is not the focus of this work.

Heterogeneous Long-Lived States in Free NFκB. The smFRET traces were further characterized as stable (82% of the traces) or fluctuating (18% of the traces) (Fig. 2*C*, S6-32). A stable trace was defined as containing long-lived state(s) with lifetimes longer than the photobleaching lifetime in that trace, which averages 90 sec (Fig. S1). In most stable traces, the single NFκB molecules spent the entire observation time in one long-lived state until photobleaching. In long-lived states, there is no anticorrelation between donor and acceptor signals (Fig.S2). A broad range of long-lived states with low- to mid- to high-FRET efficiencies were all observed (Fig. 2*E, S6-32*). Occasionally, there were transitions between two states in a trace (Fig. 2*F*), indicating these long-lived states are interconvertible via slow dynamics likely in the minutes timescale. To avoid broadening in the histogram caused by noise, a histogram for long-lived states was built by binning the mean FRET efficiency of each visit to a long-lived state (Fig. 2*D*). The histogram constructed in this way showed that these long-lived states could not be separated into a few groups amenable to hidden Markov modeling. Instead, we observed a heterogeneous, continuous distribution. A continuum of long-lived states and transitions between

them were still observed in the presence of DTT, indicating that the heterogeneity was not caused by formation of disulfide bonds (Fig. S3).

DNA binding shifts the distribution of Long-Lived States. To investigate how DNA-binding affects the relative positions and the motions of the two NTDs, we carried out smFRET experiments with NFκB bound to a biotinylated hairpin DNA containing the IFN κB binding site which was immobilized on the passivated surface through biotin-NeutrAvidin interactions (Fig. 3*A*). By immobilizing through biotinylated DNA, we ensured that every NFκB molecule we observed is DNA-bound. We collected 199 smFRET traces for DNA-bound NFκB, of which 84% could be categorized as stable—containing long-lived state(s) with lifetimes longer than the photobleaching lifetime. (Fig. S1, S33-43). Surprisingly, DNA did not shift the conformational ensemble to a single high-FRET state as expected from the crystal structure (Fig. 2*A*), but instead shifted the distribution of long-lived states to a distribution of populations which included a high-FRET population in good agreement with the crystal structure as well as an unexpected low-FRET population (Fig. 3*B,C*). Traces in which molecules sampled a distribution of mid-FRET states were also observed (Fig. 3*E,* S33-43). As was the case for free NFκB, transitions between states were captured, indicating the long-lived states could also convert to other states in DNA-bound NFκB likely via dynamics on the minutes timescale (Fig. 3*F*).

Since all crystal structures of DNA-bound NFκB indicate a ~30 Å distance between the labeling positions (PDB entries: 1VKX, 1LE5, 1LE9, 1LEI, 2I9T, 2O61, and 3GUT), it is surprising to observe a major population at low FRET efficiency. A crystal structure of NFκB p50 homodimer bound to two double-stranded RNA molecules (21) suggested that the observed low FRET state could be caused by binding to two DNA molecules on the surface of the microscope slide. To test this possibility, we carried out smFRET titration experiments, this time immobilizing the NFκB and adding a range of DNA concentrations (Fig. 3*G*). If the low-FRET state was a conformation caused by binding to two DNA molecules, the relative peak height for the low-FRET population would be expected to increase with the DNA concentration. It is important to note that because the NFκB is immobilized, we expect a population of free NFκB to contribute to the histogram. The results showed that a range of NFκB:DNA molar ratios from 10:1 to 1:100 lead to almost identical FRET histograms built by counting the first 10 seconds. Each histogram appears to have two slightly higher peaks at high and low FRET efficiencies contributed by DNA-bound NFκB superimposed on the broad distribution expected from free NFkB (Fig. 3*G*). The independence of the FRET histogram on the DNA concentration suggests that the low-FRET state was not a conformation resulting from binding to two copies of DNA but is likely a conformation with one NTD dissociated from DNA.

We turned to coarse-grained AWSEM simulations (14, 22) to understand whether NFκB bound to one copy of DNA could adopt a state in which the NTDs were farther apart leading to low FRET. Indeed, constant temperature simulations revealed a similar broad distribution in distances between labeling positions with a major population with ~30 Å distance as in the crystal structure and another major population with a larger distance leading to lower FRET (Fig. 3*D*).

Relative domain motions on the seconds timescale. Besides the stable traces observed for free NFκB, 17% of the smFRET traces were categorized as fluctuating (Fig. 2*C,* S28-32), based on the occurrence of several transitions between different states during the observation time. These transitions had anticorrelated donor and acceptor signals resulting in fluctuations in FRET efficiency indicative of relative motions between the two domains. In some traces, the motions were large enough to connect low- and high-FRET states, corresponding to a 70 Å to 30 Å inter-dye distance change (Fig. 4*A*). The motions displayed a high level of heterogeneity and, as was the case for the long-lived states, the motions could not be described by a few discrete states. In other traces (Fig. 4*B*), the two domains fluctuated around a low-FRET state (FRET efficiency ~0.25, distance ~60 Å), and then transitioned to a high-FRET state (FRET efficiency ~0.8, distance ~40 Å) and fluctuated around that value. We also observed that NFκB molecules transitioned from a fluctuating state to a long-lived state where they could be temporarily trapped (Fig. 4*C*). This again confirmed the long-lived states are not static but are interconvertible with other shorter-lived conformational states. The traces that were categorized as fluctuating were subjected to cross-correlation analysis for the donor and acceptor signals. The cross-correlation

monotonically decayed as a function of time, suggesting no periodicity for the relative domain motions, and reflecting the stochastic diffusion-like dynamics of single protein domains (Fig. 4*G*). The cross-correlation could be fitted with bi-exponential functions giving decay rates for free NFκB of 2.0 ± 0.3 s^{-1} and 0.12 ± 0.01 s^{-1} and amplitudes of 22 ± 2 and 38 ± 1 respectively. Characteristic fluctuation times, defined as the reciprocal of the rates, were 0.5 seconds and 8.4 seconds for free NFκB. We also examined the effect of ionic strength on the domain motions. A series of smFRET experiments with NaCl concentrations from 100 mM to 250 mM showed that the percentage of fluctuating traces (Fig. S4*A*) and fluctuating time scale (Fig. S4*B*) are dependent on ionic strength but not with a monotonic trend.

Fluctuation Times for DNA-Bound NFκB. NFκB bound to immobilized DNA also showed fluctuations on the seconds timescale. However, large-scale fluctuations connecting low- and high-FRET states were no longer observed (Fig. 4*D*, *E,* S44-46). As in free NFκB, DNA-bound NFκB also transitioned between fluctuating states and long-lived states (Fig. 4*F*). Cross-correlation analysis of DNA-bound NFκB traces categorized as fluctuating yielded decay rates of 1.1 ± 0.2 s^{-1} and 0.06 ± 0.01 s^{-1} and amplitudes of 11 ± 1 and 8.4 ± 0.6 respectively. The corresponding fluctuation times were 0.9 seconds and 17 seconds. The smaller amplitudes reflect the lack of fluctuations connecting low- and high-FRET states. Both times are two-fold slower than those for free NFκB. The decreased fluctuation amplitudes and rates for DNA-bound NFκB are expected from the additional intermolecular interactions introduced by the negatively charged DNA.

IκBα Locks the NFκB Domain Motions through the PEST sequence. To investigate how the inhibitory protein, IκBα, that strips NFκB from DNA and prevents DNA rebinding affects the relative domain motions of NFκB, we carried out smFRET experiments for IκBα-bound NFκB. For these experiments, non-tagged RelA-p50 dimer was used and IκBα was immobilized via a N-terminal His-tag (Fig. 5*A*). The FRET histogram constructed from 168 traces showed that every IκBα-bound NFκB populated a stable low-FRET state (Fig. 5*B, E,* S47-57). The histogram built by counting each visit to a long-lived state revealed a narrow conformational distribution in the range of 0.1 to 0.4 FRET efficiency (56 to 74 Å inter-dye distance) (Fig. S5A). All traces contained long-lived states with lifetime longer than the photobleaching lifetime. No anticorrelation of donor and acceptor signals were observed (Fig. S2C), suggesting the relative domain motions displayed in free and DNA-bound NFκB were completely suppressed by IκBα. Transitions between long-lived states were not observed either. The results show that IκBα reduced the conformational heterogeneity and locked the domain motions to a stable low-FRET state.

We next performed the same experiment for NFκB bound to the 5xPEST IκBα mutant, which contains charge-neutralizing mutations E282Q/E284Q/D285N/E286Q/E287Q in the C-terminal disordered PEST sequence and is impaired in its molecular stripping function (Fig. 5*C*) (13). Our smFRET results showed that, in contrast to wildtype, 5xPEST IκBα was not able to lock the NFκB domain motions to a stable low-FRET state. Instead, 5xPEST IκBα-bound NFκB displayed a broad distribution of long-lived states and domain fluctuations as was observed in free NFκB (Fig. 5*D, F,* S58-64). Interestingly, we observed relatively more fluctuating traces in 5xPEST IκBα-bound NFκB, which implies that placing a charge-neutral polypeptide in between the NFκB NTDs may reduce the electrostatic interactions that may lead to long-lived states. Our results show that the stripping and inhibitory function of IκBα is related to its ability to lock the NFκB NTDs in a fixed position, and that this function requires the negative charges on the IκBα PEST sequence.

Discussion

Our smFRET results suggest a hierarchical rugged energy landscape for NFκB, with many deep wells leading to long-lived conformational states interconvertible on the minutes timescale superimposed on a rough surface of substates that interconvert on the seconds timescale. In contrast to a more accepted picture of conformational switching between just a few states, NFκB appears to adopt a large number of conformations that constitute the continuous distribution observed by smFRET.

We are unaware of any previous reports of such extremely slow and heterogenous dynamics for a protein system. The continuous conformational distribution of NFκB spanning nanometers in distance resembles the continuous nature of conformational ensembles of intrinsically disordered proteins without any tertiary structures. In the case of NFκB, the flexible interdomain linker could lead to stochastic diffusion of the domains as they constantly reposition and reorient. However, motions due to diffusion are typically fast and cannot explain the extremely slow conformational dynamics observed in NFκB.

One explanation for slowed motions is electrostatic interactions between domains. The non-uniform charge distribution in NFκB domains could drive relative motions between them as a result of balancing attractive and repulsive interactions. An analysis of the electrostatic potential of the RelA-p50 heterodimer revealed electrostatic repulsion between the NTDs as well as attraction between the NTD and the DD of p50, which could drive the large-scale conformational change from a closed to an open state (5). Electrostatic interactions between domains could also stabilize interfaces formed in their transient interactions, leading to the long-lived states observed in smFRET. The frustration between the many options for attractive and repulsive long-range electrostatic interactions among the protein domains could lead to slow large-scale relative motions. Indeed, varying the ionic strength altered the interdomain motions, and addition of the negatively charged DNA caused the motions to be even slower and of reduced amplitude. The comparison between wild type and 5xPEST IκBα with a charge-neutral PEST also suggest that elimination of the conformational heterogeneity and dynamics is achieved through the highly negatively charged PEST sequence and placing a charge-neutral polypeptide in between the NFκB NTDs reduces the electrostatic interactions leading to heterogeneous long-lived states, consistent with our hypothesis that the slow heterogeneous dynamics originated from electrostatic frustration.

Besides electrostatics, linker rigidity might also cause the conformational dynamics to be slow. The highly conserved 10-amino-acid linker of NFκB subunits contains a proline and several charged residues, with the sequence DNRAPNTAEL for RelA and DSKAPNASNL for p50. Prolines and charged residues are known to increase the rigidity of disordered linkers (23) and proline isomerization additionally may contribute to the slow domain motions we observed.

The observation that DNA-bound NFκB populates a continuous density of states seems to contradict the NFκB-DNA crystal structure. However, it has been reported that despite the compact conformations observed in crystal structures, large-scale domain motions on the μs to ms timescale were observed for the 627-NLS domain of the PB2 segment of influenza polymerase by NMR, SAXS, and smFRET (24). Another multidomain protein, the human U2AF65 spliceosome assembly factor was also reported to sample a continuum of different conformations by NMR and SAXS (25).

A rugged energy landscape can be very useful in signaling, in which efficiency and reversibility of macromolecular interactions are important. Conformational flexibility could enable functional versatility of a protein. In the case of NFκB, the heterogenous long-lived states and the domain fluctuations on the seconds timescale could both be useful in controlling DNA association. To understand the relationship between NFκB dynamics and DNA binding, we compare the timescales of binding and conformational dynamics. The average time needed for a DNA binding event can be estimated from the known rate constant (k_{on}) 2.7×10^{8} $M^{-1}s^{-1}$ (5) and the estimated nuclear concentration of κB sites (1-100 nM). By calculating $1/([\kappa B\ sites]\times k_{on})$ we obtain 0.1 – 10 seconds for a binding event. Recent *in vivo* single-molecule imaging showed that the binding time of RelA to DNA is in the same range (26). The observed long-lived states typically have lifetimes longer a minute and thus can be considered static from the viewpoint of DNA-binding. These long-lived states consist of a broad distribution of the positioning of the NTDs with respect to each other. It is likely that only some of them are the “open conformations” with binding cavities accessible for DNA. By partitioning the long-lived states, NFκB could control the proportion of molecules accessible to DNA. Besides, the domain motions characterized by fluctuation times 0.5 and 8.4 seconds are on the same timescale as the DNA-binding events are. While the minutes motions may be used as a static control, the seconds motions are coupled to DNA-binding and could be a dynamics control in which the re-orientation of NTDs during the

binding process, from first encountering DNA to forming a bound complex, affects the DNA-association kinetics.

NFκB domain motions not only could control DNA-binding but also could be important for its dissociation from DNA. Transcription factor binding to DNA and dissociation from DNA are the two time points defining the transcription time window, which controls the amount of mRNA produced (27). In the NFκB-DNA-IκBα signaling network, we have previously shown that cessation of transcription occurs by IκBα-induced dissociation of NFκB from DNA (28), or "molecular stripping" (14). Molecular stripping starts when IκBα encounters NFκB bound to DNA and involves formation of a transient IκBα-NFκB-DNA ternary complex (12). Finally, DNA dissociates and is unable to rebind the remaining NFκB-IκBα complex (13). With molecular stripping, the DNA dissociation rate is proportional to and thus controlled by the IκBα concentration. Just as the broad distribution of motional timescales in free NFκB can be useful to control DNA binding, those in NFκB-DNA may control the binding of IκBα to initiate molecular stripping. Previous coarse-grained MD simulations suggest that IκBα induces a twist in the NTDs during molecular stripping so that only one NTD can make contacts with the DNA, lowering the barrier for DNA dissociation (15). With smFRET, we observed that IκBα locked the NFκB NTDs in a static low-FRET state consistent with twisting and spreading away from a DNA-binding competent state. The remaining conformational dynamics in NFκB bound to the stripping impaired 5xPEST IκBα showed that reorientating the NTDs to a static state is required for molecular stripping. The fact that the IκBα-bound NFκB is the only static state we observed also strongly suggests that NTD motions are required for DNA-binding. Our results suggest that both functions of IκBα, molecular stripping and preventing DNA-binding, come from altering the NFκB NTD motions. By reorienting the NTDs, IκBα lowers the DNA dissociation barrier, and by eliminating the conformational heterogeneity, IκBα inhibits NFκB-DNA interactions. In conclusion, the extremely slow and heterogenous NFκB NTD motions observed by smFRET reveal a rugged energy landscape that can be reshaped by DNA and IκBα. NFκB adopts a continuous distribution of conformations that were completely unexpected based on previously reported crystal structures. We propose that the observed domain motions control the association and dissociation of NFκB and DNA to achieve efficient transcription activation and allow IκBα to efficiently terminate transcription.

Materials and Methods

Protein expression, purification, and labeling. Plasmids of murine $RelA_{1-325}$ (UniProt entry Q04207) and $p50_{39-363}$ (UniProt entry P25799) in pET11a vectors (Plasmid #44744, Addgene) were provided by Gourisankar Ghosh at UCSD. A 6xHis-tag was introduced to the C-terminus of RelA by site-directed mutagenesis for immobilization. Q128 of RelA and F148 of p50 were mutated into Amber stop codons TAG by site-directed mutagenesis for unnatural amino acid incorporation and fluorophore labeling. Plasmid containing RelA or p50 was co-transformed with pEVOL-pAzF (Plasmid #31186, Addgene), the plasmid encoding the aaRS/tRNA pair for incorporating the unnatural amino acid p-azidophenylalanine (pAzF, CAS 33173-53-4, Chem-Impex Int'l. Inc.), into BL21 (DE3) *E. coli* strain (New England Biolabs). Cells were first grown in M9 minimal media with 200 mg/L ampicillin and 34 mg/L chloramphenicol at 37 °C and 180 rpm. At 0.6 - 0.7 OD_{600}, the expression of RelA or p50 was induced with 0.2 mM IPTG, and the expression of the aaRS/tRNA was induced with 0.02% L-arabinose. pAzF was added to a 200 mg/L final concentration. Cells were then grown at 18 °C and 180 rpm for 16 hours and harvested by centrifugation at 5,000 rcf for 15 minutes. The cell pellet containing His-tagged RelA was resuspended in 50 mM sodium phosphate pH 8, 150 mM NaCl, 10 mM imidazole, 0.5 mM PMSF with protease inhibitor cocktail (Sigma-Aldrich). Following sonication on ice, the cell lysate was centrifuged at 17,000 rcf for 30 minutes. The supernatant was passed through Ni-NTA resins (Thermo Fisher Scientific) and washed with 10 column volumes of the wash buffer (50 mM sodium phosphate pH 8, 150 mM NaCl, 20 mM imidazole). RelA was eluted with 50 mM sodium

phosphate, 150 mM NaCl, 250 mM imidazole. Elution was pass through a PD 10 desalting column (GE Healthcare) to remove imidazole and eluted with 25 mM Tris pH 7.5, 150 mM NaCl, 0.5 mM EDTA. After added the protease inhibitor cocktail and glycerol (5% final concentration), the sample was aliquoted and stored at -80 °C for further fluorophore labeling and purification. The cell pellet containing non-tagged RelA or p50 was resuspended in 25 mM Tris pH 7.5, 150 mM NaCl, 0.5 mM EDTA, 0.5 mM PMSF. After sonication and centrifugation, the supernatant was passed through SP Sepharose Fast Flow resins (GE Healthcare). An NaCl gradient from 0 to 700 mM NaCl was used to elute the protein. The elution fraction was purified with a PD10 desalting column and stored in 20 mM Tris pH7.5, 150 mM NaCl, 0.5 mM EDTA, 5% glycerol at -80 °C. Reducing agents was avoided to prevent reducing pAzF to pAmF (p-aminophenylalanine). Expression of full-length $RelA_{1-325}$ and $p50_{39-363}$ was confirmed by SDS-PAGE. Site-specific incorporation of pAzF was further confirmed by pepsin digestion and tandem mass spectrometry. Peptides DLE*AISQR (M+H 1093.567, residues 126 – 133 of RelA) and GILHVTKKKV*ETL (M+H 1653.984, residues 138 – 161 of p50) containing pAzF (denoted by asterisk) were identified. Fluorophore labeling was achieved through the copper-free click reaction between the azido sidechain of the incorporated pAzF and the sDIBO functional group on the fluorophore. RelA and p50 were thawed from -80 °C and labeled separately with Click-iT™ Alexa Fluor™ 555 sDIBO Alkyne (FRET donor, Thermo Fisher Scientific) or Click-iT™ Alexa Fluor™ 647 sDIBO Alkyne (FRET acceptor, Thermo Fisher Scientific) with a 1:2 protein-to-dye molar ratio at 4 °C for 2-7 days. The FRET radius R_0 of the donor/acceptor pair used in this study is 51 Å. Excess dyes were removed with PD10 desalting columns. Labeling efficiency was determined with the extinction coefficients (ε^{RelA}_{280} = 20,400 M^{-1} cm^{-1}, ε^{p50}_{280} = 23,380 $M^{-1}cm^{-1}$, $\varepsilon^{Alexa555}_{555}$ = 155,000 $M^{-1}cm^{-1}$, $\varepsilon^{Alexa647}_{650}$ = 239,000 $M^{-1}cm^{-1}$) and the correction factors accounting for A280 from the dyes ($CF_{Alexa555}$ = 0.08, $CF_{Alexa657}$ = 0.03). The labeling efficiency is 29% to 56 % for Alexa Fluor 555 to RelA, 20% to 35% for Alexa Fluor 647 to RelA, 52% to 83% for Alexa Fluor 647 to p50, and 18% to 50% for Alexa Fluor 647 to p50. Labeled RelA and p50 were mixed with a 1:5 donor:acceptor molar ratio to form RelA-p50 heterodimer. The dual-labeled heterodimer was then purified by cation exchange chromatography (Mono S 10/100, GE Healthcare) in 25 mM Tris pH 7.5, 0.5 mM EDTA, 1mM DTT with an NaCl gradient from 100 to 700 mM and size exclusion chromatography (Superdex 200, GE Healthcare) in Tris pH 7.5, 150 mM NaCl, 0.5 mM EDTA, 1mM DTT as previously used for wildtype RelA-p50 heterodimer (28).

Human $I\kappa B\alpha_{67-287}$ (Uniprot entry P25963) in pET11a was introduced with a N-terminal 6xHis tag. The 5xPEST IκBα had the following mutations: E282Q/E284Q/D285N/E286Q/E287Q and was expressed and harvested as previously described for nontagged IκBα (29). Cell lysates were passed through Ni-NTA resin equilibrated in buffer A (25 mM Tris pH 7.5, 150 mM NaCl, 10 mM imidazole, 10 mM βME), washed with wash buffer (25 mM Tris pH 7.5, 150 mM NaCl, 20 mM imidazole, 10 mM βME), and eluted with buffer B (25 mM Tris pH 7.5, 150 mM NaCl, 250 mM imizadole, 10 mM βME). Fractions containing IκBα were then dialyzed overnight at 4°C in SEC buffer containing 25 mM Tris pH 7.5, 150 mM NaCl, 0.5 mM EDTA, 1mM DTT. The dialyzed protein was then either frozen in 2 mL aliquots at −80°C until needed or immediately further purified from aggregates by size exclusion chromatography (Superdex S75; GE Healthcare) in SEC buffer. The IκBα concentration was determined with the extinction coefficient $\varepsilon^{I\kappa B\alpha}_{280}$ = 12,950 M^{-1} cm^{-1}

Single-molecule FRET data collection. A prism-type total internal reflection fluorescence (TIRF) microscopy was used. For Alexa Flour 555/ Alexa Flour 647 dye pair, a 532 nm laser (SAPPHIRE 532-300 CW CDRH, Coherent) and a 637 nm laser (OBIS™ 1196625 | 637nm LX 140mW Laser, Coherent) were set up to excite donor and acceptor respectively. Laser output powers were set to 50 mW for smFRET experiments. 532 nm and 637 nm laser beams were guided by mirrors and a beam splitter to colocalize on the excitation area on the prism. An inverted microscope was set up by mounting the objective (CFI Plan Apochromat VC 60XC WI, Nikon) on a Rapid Automated Modular Microscope System (Applied Scientific Instrumentation). Emission light was further split into donor and acceptor channels with a DV2 Two-Channel, Simultaneous-Imaging System (Photometrics) with band pass filters (ET585/65m for donor channel and ET685/56m for acceptor channel, Chroma). Fluorescent signals were detected by

Electron Multiplying Charge-Coupled Device (EMCCD) (iXonEM+ EMCCD camera, DU-897E-CS0-#BV, Andor Technology). DDS-Tween 20 passivated surface (19) with 0.2 mg/mL biotinylated bovine serum albumin (A8549, Sigma-Aldrich) and 0.2 mg/mL NeutrAvidin (31000, Thermo Fisher Scientific) were used to immobilize NFκB. For free NFκB experiments, NFκB molecules were immobilized through the 6xHis-tag on the C-terminus of RelA by penta-His antibody biotin conjugate (34440, Qiagen). For DNA-bound NFκB experiments, DNA-NFκB complexes were immobilized through the biotinylated hairpin DNA containing the underlined κB sequence:

Biotin-GCATGCGGGAAATTCCATGCATGCCCCCCATGCATGGAATTTCCCGCATGC

For IκBα-bound NFκB experiments, IκBα-NFκB complexes were immobilized through the 6xHis-tag on the N-terminus of IκBα.

Experiments were performed at room temperature in imaging buffer (25 mM Tris pH 7.5, 150 mM NaCl, 0.5 mM EDTA, 0.8 mg/mL glucose oxidase (G2133, Sigma-Aldrich), 0.2 mg/mL catalase (219001, CALBIOCHEM), 0.4% dextrose, and 5 mM Trolox (CAS 53188-07-1, Sigma-Aldrich)). Trolox was prepare by dissolving 10 mg Trolox powder in 10 mL of 25 mM Tris, pH 7.5, 150 mM NaCl, 0.5 mM EDTA with vortexing for 30 minutes and then incubation at room temperature and ambient light overnight. The 637 nm laser was used to confirm the existence of acceptor fluorophores and the 532 nm laser was used for excitation of the donor fluorophore. Data acquisition and analysis software was obtained from the Ha Lab at Johns Hopkins University http://ha.med.jhmi.edu/resources/#1464200861600-0fad9996-bfd4. Single molecule movies were recorded with 100 ms time resolution.

Single-molecule FRET data analysis. Individual single-molecule traces were extracted from the acquired movies with the IDL scripts in the Ha Lab software package. The traces were further selected based on the criteria: (i) clear single photobleaching step for both donor and acceptor; (ii) anticorrelation pattern for donor and acceptor intensities; (iii) stable total fluorescence intensity before photobleaching; (iii) > 10 sec photobleaching lifetime for both donor and acceptor. Time periods with no signals caused by donor or acceptor dark states, an unbound state, or a state in which an unlabeled NFκB is bound to the immobilized DNA or IκBα were excluded. For each trace, background was defined as the mean values of the donor and acceptor fluorescence intensities after photobleaching and subtracted from the data. To account for the donor signal leakage to the acceptor channel, we measured the correction factor by collecting data of Alexa Flour 555 labeled RelA. After background subtraction for individual traces of Alexa Flour 555 labeled RelA, the correction factor was defined as the mean value of the ratio of the acceptor intensity to the donor intensity and calculated to be 0.04. Therefore, for a single-molecule trace, the background and donor leakage are corrected by the following equation in which I is the fluorescent intensity:

$$I_{donor} = I_{donor}^{raw} - I_{donor}^{background}$$
$$I_{acceptor} = I_{acceptor}^{raw} - I_{acceptor}^{background} - 0.04 \times I_{donor}$$

The FRET efficiency (E) was calculated using the corrected fluorescent intensities. $E = I_{acceptor} / (I_{donor} + I_{acceptor})$. Finally, traces were categorized as fluctuating based on whether the signal fluctuations were larger than that caused by noise (shown in the signal after photobleaching). Traces with no fluctuations larger than noise were categorized as stable.

FRET data were presented in two types of histograms. In the first type, the first 1000 timepoints (10 seconds) of each trace were used as data points to build the histogram. In the second type, fluctuating traces were not included, and mean FRET efficiency values of each individual long-lived state were used as data points to build the histogram. The first type of histogram built by counting timepoints is useful for general purposes and the second type built by counting visits to long-live states eliminated noise and was used to show the continuous distribution of states.

Fluctuating traces were subjected to cross-correlation analysis. The cross-correlation function is defined as previously described (30). Only traces longer than 30 seconds were included in the analysis and the correlation up 15 seconds were calculated. Results were fitted with a bi-exponential function to compare the characteristic fluctuation time.

Molecular simulations and analysis. We used OpenAWSEM (22) to model the heterodimer-DNA complex. The initial structures of the protein and DNA were from the crystal structure of NFkB (PDB entry: 1LE5). We extended the DNA sequence 100 pairs of A/T at both ends to reduce any finite size effect caused by having a short DNA sequence. The protein and DNA were initially placed far away from each other. Chain A (RelA) of the protein was shifted 300 Å to the left along the x axis from the DNA and chain B (p50) was shifted 300Å to the right. As the simulation began, both chains of the protein were pulled toward the DNA with a native protein-DNA contact bias. This bias was turned off after 10 million steps. Then, we ran another 10 million steps of unbiased simulation. We used a Langevin integrator with a friction of 1 ps^{-1} and a step size of 2 fs. The simulations were carried out at constant temperature of 300 K. The default strength for each term followed our previous study (15), with $V_{contact}$=0.75, V_{HB}=0.5. We did not use a Gō term in this study. The fragment memory consisted of nine equally weighted structures. Among them, one was the crystal structure, and the other 8 structures are sampled from two independent all-atom simulations (5) at 100, 200, 300, and 400 ns. The simulations were repeated 20 times with the same initial structures but different initial velocities and different random seeds. The trajectories were saved every 4000 steps and the last 2000 frames were used for analysis.

Acknowledgments
The authors thank Hajin Kim at Ulsan National Institute of Science and Technology for his advice on setting up the TIRF microscope, Majid Ghassemian at the Biomolecular and Proteomics Mass Spectrometry Facility, UCSD for carrying out the mass spectrometry analyses, and Andy McCammon for helpful discussions. W.C. acknowledges fellowship support from the Taiwanese Ministry of Education.

References
1. J. H. Han, S. Batey, A. A. Nickson, S. A. Teichmann, J. Clarke, The folding and evolution of multidomain proteins. Nat Rev Mol Cell Biol 8, 319-330 (2007).
2. R. G. Smock, L. M. Gierasch, Sending signals dynamically. Science 324, 198-203 (2009).
3. G. D. Amoutzias, D. L. Robertson, Y. Van de Peer, S. G. Oliver, Choose your partners: dimerization in eukaryotic transcription factors. Trends Biochem Sci 33, 220-229 (2008).
4. D. Vuzman, M. Polonsky, Y. Levy, Facilitated DNA search by multidomain transcription factors: cross talk via a flexible linker. Biophys J 99, 1202-1211 (2010).
5. D. Narang, W. Chen, C. G. Ricci, E. A. Komives, RelA-Containing NFkappaB Dimers Have Strikingly Different DNA-Binding Cavities in the Absence of DNA. J Mol Biol 430, 1510-1520 (2018).
6. E. B. Traenckner, P. A. Baeuerle, Appearance of apparently ubiquitin-conjugated I kappa B-alpha during its phosphorylation-induced degradation in intact cells. J Cell Sci Suppl 19, 79-84 (1995).
7. R. Martone, G. Euskirchen, P. Bertone, S. Hartman, T. E. Royce, N. M. Luscombe, J. L. Rinn, F. K. Nelson, P. Miller, M. Gerstein, S. Weissman, M. Snyder, Distribution of NF-kappaB-binding sites across human chromosome 22. Proc Natl Acad Sci U S A 100, 12247-12252 (2003).
8. A. Hoffmann, A. Levchenko, M. L. Scott, D. Baltimore, The IkappaB-NF-kappaB signaling module: temporal control and selective gene activation. Science 298, 1241-1245 (2002).
9. F. Arenzana-Seisdedos, P. Turpin, M. Rodriguez, D. Thomas, R. T. Hay, J.-L. Virelizier, C. Dargemont, Nuclear localization of I kappa B alpha promotes active transport of NF-kappa B from the nucleus to the cytoplasm. Journal of cell science 110, 369-378 (1997).
10. T. Huxford, D.-b. Huang, S. Malek, G. Ghosh, The crystal structure of the IκBα/NF-κB complex reveals mechanisms of NF-κB inactivation. Cell 95, 759-770 (1998).
11. M. D. Jacobs, S. C. Harrison, Structure of an IκBα/NF-κB complex. Cell 95, 749-758 (1998).
12. V. Alverdi, B. Hetrick, S. Joseph, E. A. Komives, Direct observation of a transient ternary complex during IkappaBalpha-mediated dissociation of NF-kappaB from DNA. Proc Natl Acad Sci U S A 111, 225-230 (2014).

13. H. E. Dembinski, K. Wismer, J. D. Vargas, G. W. Suryawanshi, N. Kern, G. Kroon, H. J. Dyson, A. Hoffmann, E. A. Komives, Functional importance of stripping in NFkappaB signaling revealed by a stripping-impaired IkappaBalpha mutant. Proc Natl Acad Sci U S A 114, 1916-1921 (2017).
14. D. A. Potoyan, W. Zheng, E. A. Komives, P. G. Wolynes, Molecular stripping in the NF-kappaB/IkappaB/DNA genetic regulatory network. Proc Natl Acad Sci U S A 113, 110-115 (2016).
15. D. A. Potoyan, W. Zheng, D. U. Ferreiro, P. G. Wolynes, E. A. Komives, PEST Control of Molecular Stripping of NFkappaB from DNA Transcription Sites. J Phys Chem B 120, 8532-8538 (2016).
16. B. Berkowitz, D. B. Huang, F. E. Chen-Park, P. B. Sigler, G. Ghosh, The x-ray crystal structure of the NF-kappa B p50.p65 heterodimer bound to the interferon beta -kappa B site. J Biol Chem 277, 24694-24700 (2002).
17. J. W. Chin, S. W. Santoro, A. B. Martin, D. S. King, L. Wang, P. G. Schultz, Addition of p-azido-L-phenylalanine to the genetic code of Escherichia coli. J Am Chem Soc 124, 9026-9027 (2002).
18. J. C. Jewett, C. R. Bertozzi, Cu-free click cycloaddition reactions in chemical biology. Chem Soc Rev 39, 1272-1279 (2010).
19. B. Hua, K. Y. Han, R. Zhou, H. Kim, X. Shi, S. C. Abeysirigunawardena, A. Jain, D. Singh, V. Aggarwal, S. A. Woodson, T. Ha, An improved surface passivation method for single-molecule studies. Nat Methods 11, 1233-1236 (2014).
20. B. Hellenkamp, S. Schmid, O. Doroshenko, O. Opanasyuk, R. Kuhnemuth, S. Rezaei Adariani, B. Ambrose, M. Aznauryan, A. Barth, V. Birkedal, M. E. Bowen, H. Chen, T. Cordes, T. Eilert, C. Fijen, C. Gebhardt, M. Gotz, G. Gouridis, E. Gratton, T. Ha, P. Hao, C. A. Hanke, A. Hartmann, J. Hendrix, L. L. Hildebrandt, V. Hirschfeld, J. Hohlbein, B. Hua, C. G. Hubner, E. Kallis, A. N. Kapanidis, J. Y. Kim, G. Krainer, D. C. Lamb, N. K. Lee, E. A. Lemke, B. Levesque, M. Levitus, J. J. McCann, N. Naredi-Rainer, D. Nettels, T. Ngo, R. Qiu, N. C. Robb, C. Rocker, H. Sanabria, M. Schlierf, T. Schroder, B. Schuler, H. Seidel, L. Streit, J. Thurn, P. Tinnefeld, S. Tyagi, N. Vandenberk, A. M. Vera, K. R. Weninger, B. Wunsch, I. S. Yanez-Orozco, J. Michaelis, C. A. M. Seidel, T. D. Craggs, T. Hugel, Precision and accuracy of single-molecule FRET measurements-a multi-laboratory benchmark study. Nat Methods 15, 669-676 (2018).
21. D. B. Huang, D. Vu, L. A. Cassiday, J. M. Zimmerman, L. J. Maher, 3rd, G. Ghosh, Crystal structure of NF-kappaB (p50)2 complexed to a high-affinity RNA aptamer. Proc Natl Acad Sci U S A 100, 9268-9273 (2003).
22. C. S. Sorensen, M. Kjaergaard, Effective concentrations enforced by intrinsically disordered linkers are governed by polymer physics. Proc Natl Acad Sci U S A 116, 23124-23131 (2019).
23. E. Delaforge, S. Milles, J. R. Huang, D. Bouvier, M. R. Jensen, M. Sattler, D. J. Hart, M. Blackledge, Investigating the Role of Large-Scale Domain Dynamics in Protein-Protein Interactions. Front Mol Biosci 3, 54 (2016).
24. J. R. Huang, L. R. Warner, C. Sanchez, F. Gabel, T. Madl, C. D. Mackereth, M. Sattler, M. Blackledge, Transient electrostatic interactions dominate the conformational equilibrium sampled by multidomain splicing factor U2AF65: a combined NMR and SAXS study. J Am Chem Soc 136, 7068-7076 (2014).
25. A. Callegari, C. Sieben, A. Benke, D. M. Suter, B. Fierz, D. Mazza, S. Manley, Single-molecule dynamics and genome-wide transcriptomics reveal that NF-kB (p65)-DNA binding times can be decoupled from transcriptional activation. PLoS Genet 15, e1007891 (2019).
26. N. C. Lammers, V. Galstyan, A. Reimer, S. A. Medin, C. H. Wiggins, H. G. Garcia, Multimodal transcriptional control of pattern formation in embryonic development. Proc Natl Acad Sci U S A 117, 836-847 (2020).
27. S. Bergqvist, V. Alverdi, B. Mengel, A. Hoffmann, G. Ghosh, E. A. Komives, Kinetic enhancement of NF-kappaBxDNA dissociation by IkappaBalpha. Proc Natl Acad Sci U S A 106, 19328-19333 (2009).

28. C. H. Croy, S. Bergqvist, T. Huxford, G. Ghosh, E. A. Komives, Biophysical characterization of the free IkappaBalpha ankyrin repeat domain in solution. Protein Sci 13, 1767-1777 (2004).
29. J. A. Lamboy, H. Kim, H. Dembinski, T. Ha, E. A. Komives, Single-molecule FRET reveals the native-state dynamics of the IkappaBalpha ankyrin repeat domain. J Mol Biol 425, 2578-2590 (2013).
30. W. Lu, C. Bueno, N. P. Schafer, J. Moller, S. Jin, X. Chen, M. Chen, X. Gu, A. Davtyan, J. J. de Pablo, P. G. Wolynes, OpenAWSEM with Open3SPN2: A fast, flexible, and accessible framework for large-scale coarse-grained biomolecular simulations. PLoS Comput Biol 17, e1008308 (2021).

Figures

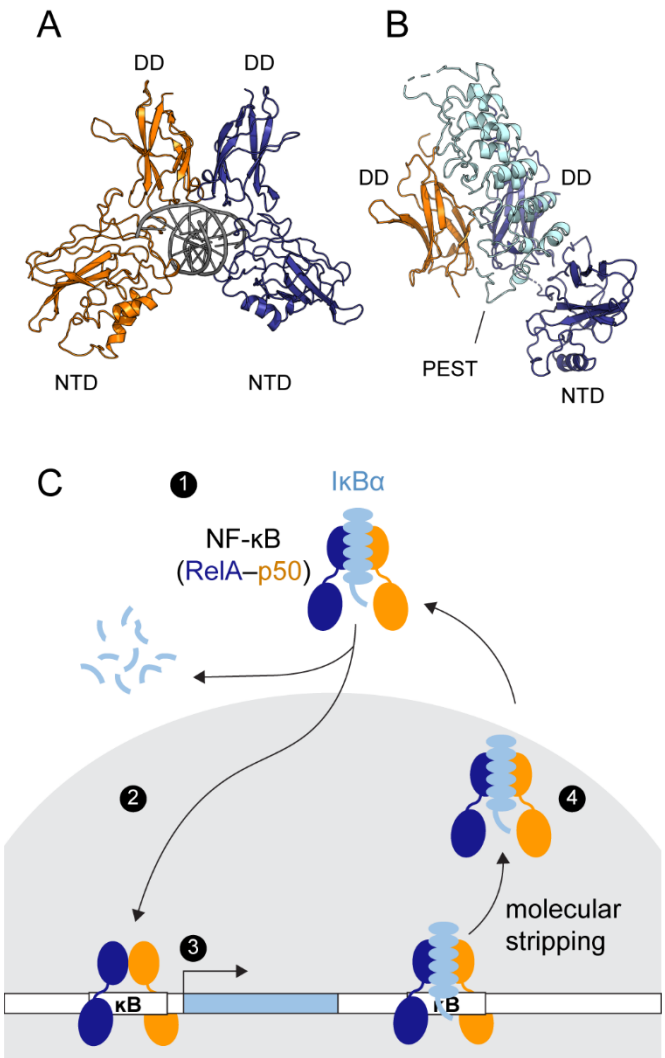

Fig. 1. Transcriptional regulation by NFκB (*A*) Structure of the NFκB RelA-p50 heterodimer bound to DNA (PDB: 1LE5, RelA in blue, p50 in orange, and DNA in grey). Each NFκB monomer contains a dimerization domain (DD) and a N-terminal DNA binding domain (NTD) connected by a 10-amino-acid linker. The NFκB dimer recognizes its cognate DNA through the two NTDs (*B*) Structure of the NFκB-IκBα complex (PDB: 1IKN, IκBα in cyan). IκBα binds to the DDs of NFκB. The disordered PEST sequence is at the C-terminus of IκBα. The NTD of p50 was truncated in order to achieve crystallization. (*C*) Schematic of NFκB transcriptional regulation showing 1) NFκB held in the cytoplasm bound to IκBα. 2) Upon signal input, IκBα is degraded freeing NFκB to enter the nucleus (grey). 3) NFκB binds to DNA and turns on hundreds of genes one of which is that for IκBα creating newly synthesized IκBα. 4) IκBα enters the nucleus and strips NFκB from the DNA returning it to the resting state.

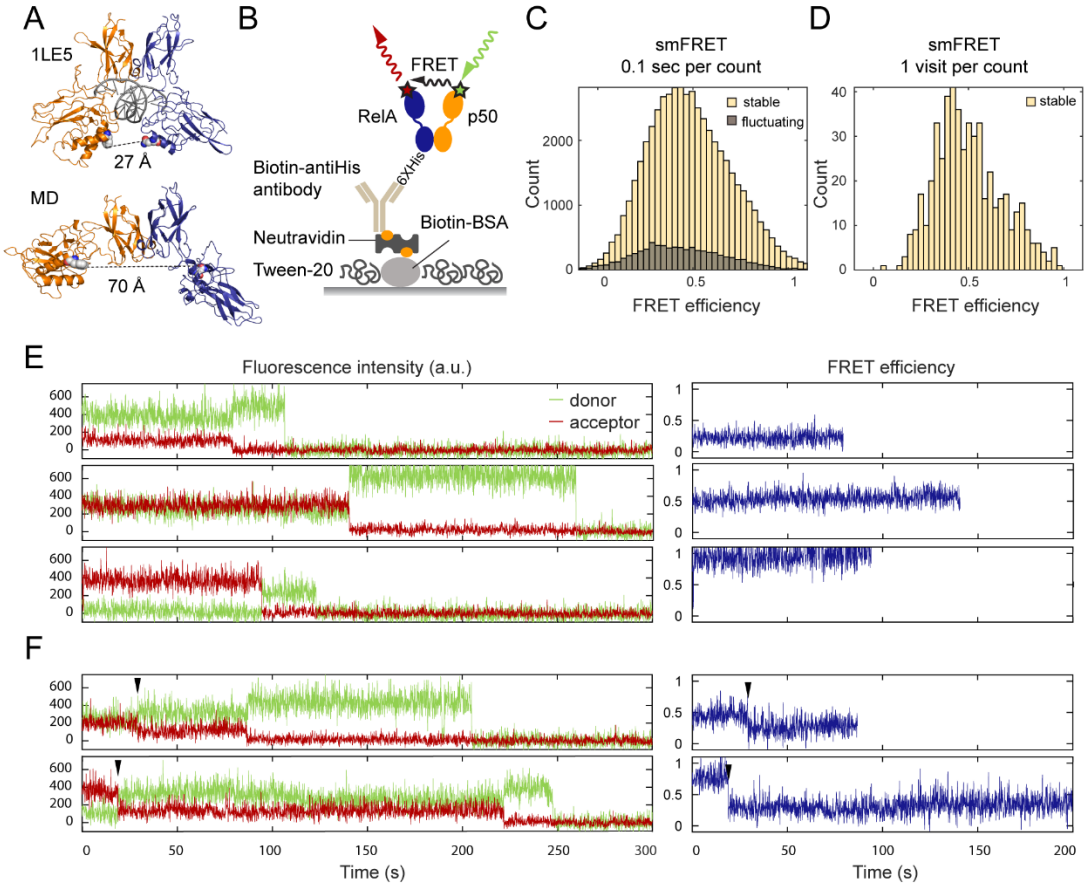

Fig. 2. smFRET experimental design for probing the relative domain motions of NFκB. (*A*) In the NFκB-DNA crystal structure (PDB: 1LE5), the distance between the two labeled positions; E128 in RelA and F148 in p50 (spheres), would lead to a high FRET efficiency ~1. In MD simulations, free NFκB could adopt an open conformation, leading to a low FRET efficiency ~0.1. (*B*) Schematic of how the NFκB (RelA-p50 dimer) was immobilized on a DT20 passivated surface via the His-tag on RelA, biotin-conjugated anti-His antibody, NeutrAvidin, and biotin-conjugated bovine serum albumin (BSA). The two NTDs were labeled with FRET donor (green star) and acceptor (red star). (*C*) Experimental FRET histogram showed a broad distribution of conformations. The histogram was constructed by counting the first 10 seconds of the traces. (*D*) Experimental FRET histogram constructed by counting each visit to a long-lived state suggested a continuous distribution of stable states that cannot be separated into a few groups. (*E*) Representative stable smFRET traces with low, mid, and high FRET efficiencies. Other long-lived states with different FRET efficiencies are shown in SI. (*F*) Transitions (arrowhead) between long-lived states were captured.

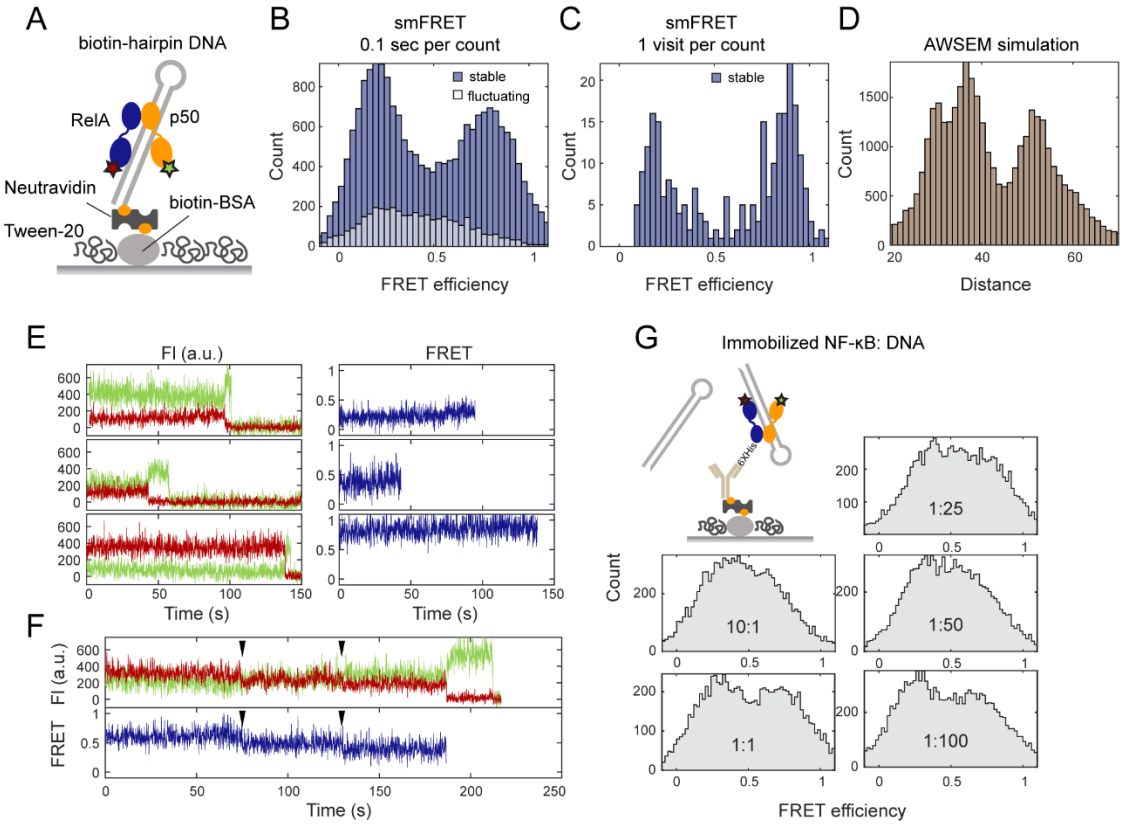

Fig. 3. smFRET experiments for DNA-bound NFκB. (*A*) Schematic of the experimental set-up. A biotinylated hairpin DNA with a κB site was used for immobilization through biotin-NreutrAvidin interactions. (*B*) FRET histogram showing two major populations at low and high FRET efficiencies contributed by stable traces. (*C*) FRET histogram constructed by counting each visit to a long-lived state showing a continuous distribution with two dominating populations. (D) Distribution of the distance between labeling positions sampled with AWSEM simulations showing two dominating populations in DNA-NFκB. (*E*) Representative stable traces showing long-lived states with low, mid, and high FRET efficiencies. (*F*) A representative trace showing transitions between long-lived states from high to mid to low FRET efficiencies. (*G*) smFRET titration experiments with immobilized NFκB and varying DNA concentrations. A series of NFκB:DNA molar ratios from 10:1 to 1:100 showed similar FRET histograms with a broad band and two slightly higher peaks at low and high FRET efficiencies.

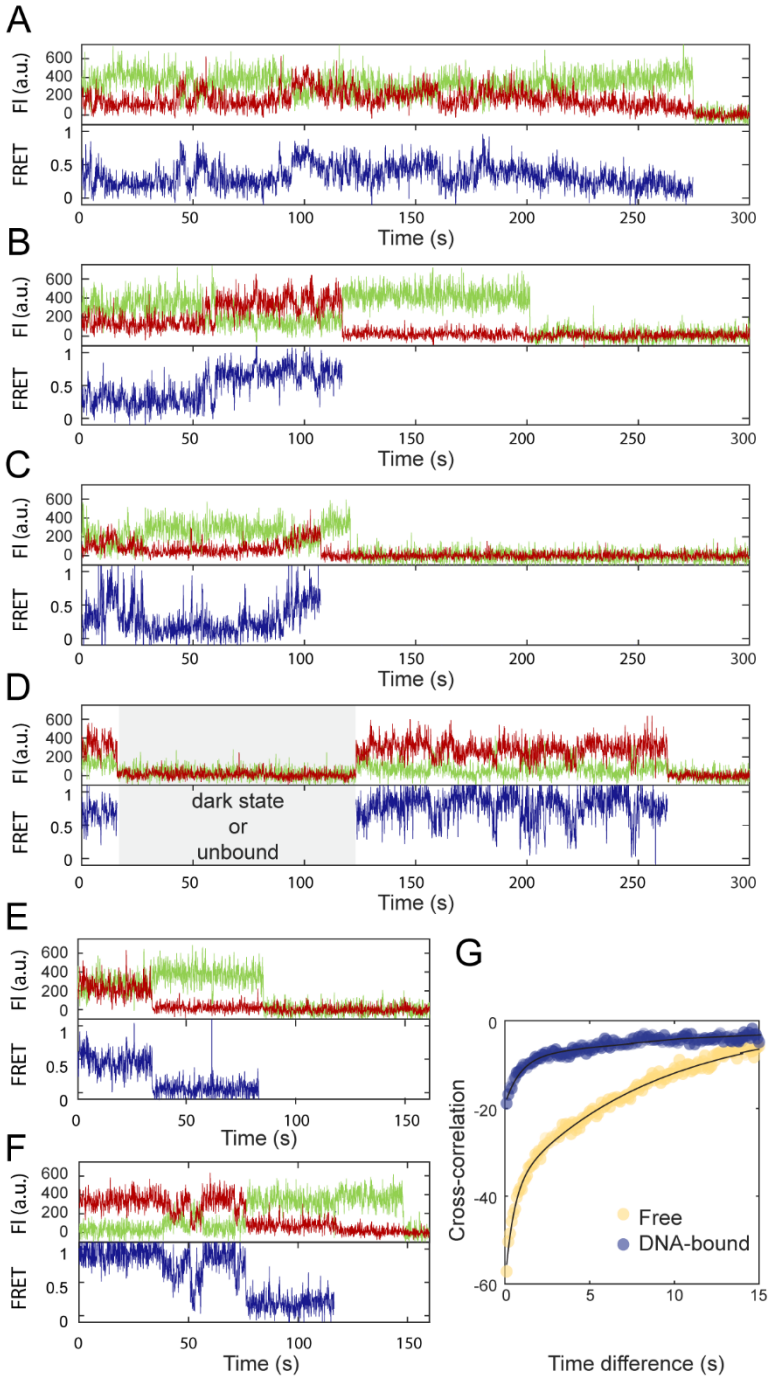

Fig. 4. Fluctuating smFRET traces of NFκB showing relative domain motions and the hierarchy of a rugged energy landscape. (*A*) Representative fluctuating traces for free NFκB with fluctuations connecting low- and high- FRET states, which corresponds 30 - 70 Å in inter-dye distance. (*B*) A trace for free NFκB with small fluctuations around a low-FRET state at first. At 60 seconds, the molecule transitioned to a high-FRET state and fluctuated around it. (*C*) A trace with transitions between fluctuations and long-lived states for free NFκB, suggesting all the conformational states are interconvertible. (*D* and *E*) Representative fluctuating traces of DNA-bound NFκB showing small fluctuations in DNA-bound NFκB. The time period with no signals (grey area) could be caused by a donor dark state, an unbound state, or a state in which an unlabeled NFκB is bound to the immobilized DNA. (*F*) A trace with transitions between fluctuating and long-lived states for DNA-bound NFκB. (*G*) Cross-correlation analyses for fluctuations of free (yellow) and DNA-bound (blue) NFκB showing that the relative domain motions of the DNA-bound NFκB have lower amplitudes and slower rates. Bi-exponential fitting revealed the characteristic fluctuation time to be 0.5 s and 8.4 s for free NFκB and 0.9 s and 17 s for DNA-bound NFκB. Dot: data; Line: fit.

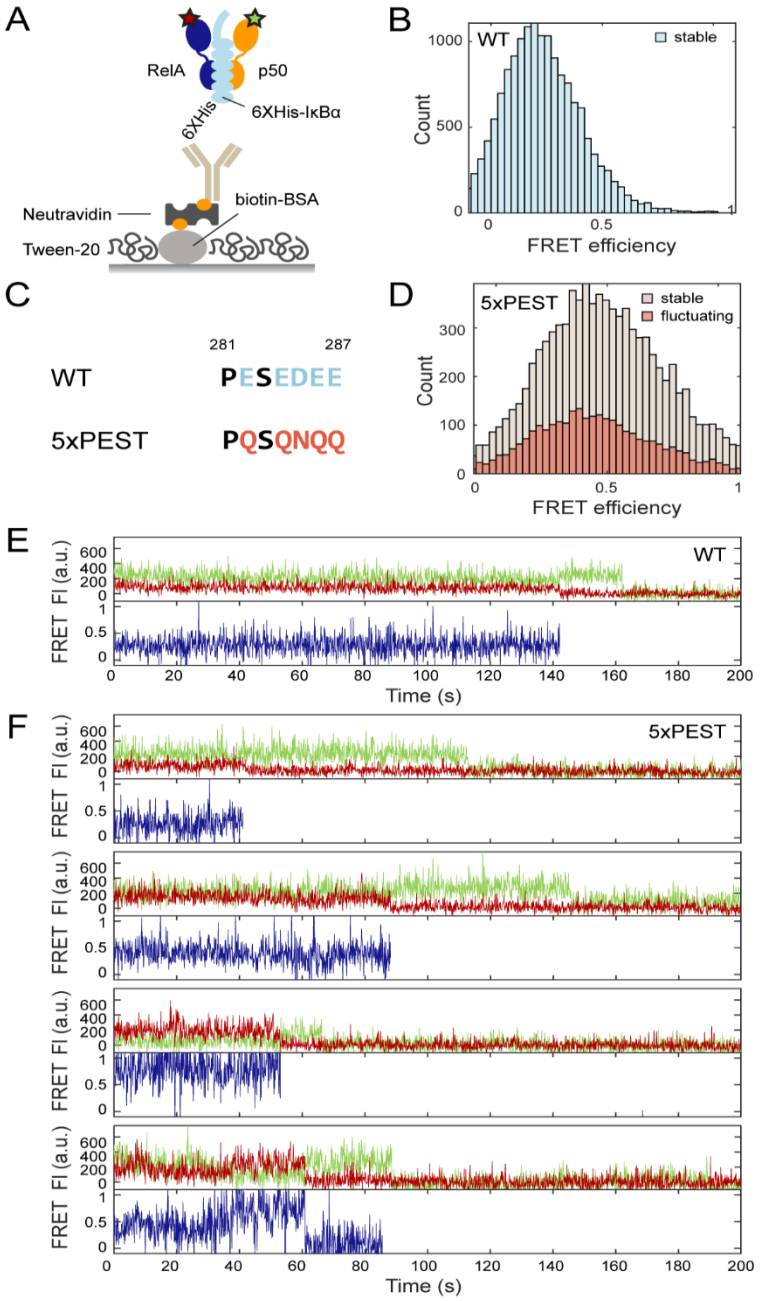

Fig. 5. smFRET experiments for IκBα-bound NFκB. (*A*) The experimental schematic. A His-tag on IκBα was used to immobilize the NFκB-IκBα complex through the interaction with anti-His antibody biotin conjugate. (*B*) FRET histogram showing the distribution of NFκB molecules bound to IκBα. Only a stable low FRET state was observed. (*C*) Five negatively charged residues in the wild type (WT) IκBα PEST sequence were mutated into neutral residues to generate the stripping impaired 5xPEST mutant. (*D*) FRET histogram for NFκB bound to the 5xPEST IκBα showing a broad distribution and a larger proportion of fluctuating traces. (*E*) A representative trace of NFκB bound to WT IκBα showing the stable low-FRET state. (*F*) Representative traces of NFκB bound to 5xPEST IκBα showing heterogeneous long-lived states with low- to mid- to high-FRET efficiencies and domain fluctuations.

1. J. H. Han, S. Batey, A. A. Nickson, S. A. Teichmann, J. Clarke, The folding and evolution of multidomain proteins. *Nat Rev Mol Cell Biol* **8**, 319-330 (2007).
2. R. G. Smock, L. M. Gierasch, Sending signals dynamically. *Science* **324**, 198-203 (2009).
3. G. D. Amoutzias, D. L. Robertson, Y. Van de Peer, S. G. Oliver, Choose your partners: dimerization in eukaryotic transcription factors. *Trends Biochem Sci* **33**, 220-229 (2008).
4. D. Vuzman, M. Polonsky, Y. Levy, Facilitated DNA search by multidomain transcription factors: cross talk via a flexible linker. *Biophys J* **99**, 1202-1211 (2010).
5. D. Narang, W. Chen, C. G. Ricci, E. A. Komives, RelA-Containing NFkappaB Dimers Have Strikingly Different DNA-Binding Cavities in the Absence of DNA. *J Mol Biol* **430**, 1510-1520 (2018).
6. E. B. Traenckner, P. A. Baeuerle, Appearance of apparently ubiquitin-conjugated I kappa B-alpha during its phosphorylation-induced degradation in intact cells. *J Cell Sci Suppl* **19**, 79-84 (1995).
7. R. Martone *et al.*, Distribution of NF-kappaB-binding sites across human chromosome 22. *Proc Natl Acad Sci U S A* **100**, 12247-12252 (2003).
8. A. Hoffmann, A. Levchenko, M. L. Scott, D. Baltimore, The IkappaB-NF-kappaB signaling module: temporal control and selective gene activation. *Science* **298**, 1241-1245 (2002).
9. F. Arenzana-Seisdedos *et al.*, Nuclear localization of I kappa B alpha promotes active transport of NF-kappa B from the nucleus to the cytoplasm. *Journal of cell science* **110**, 369-378 (1997).
10. T. Huxford, D.-b. Huang, S. Malek, G. Ghosh, The crystal structure of the IκBα/NF-κB complex reveals mechanisms of NF-κB inactivation. *Cell* **95**, 759-770 (1998).
11. M. D. Jacobs, S. C. Harrison, Structure of an IκBα/NF-κB complex. *Cell* **95**, 749-758 (1998).
12. V. Alverdi, B. Hetrick, S. Joseph, E. A. Komives, Direct observation of a transient ternary complex during IkappaBalpha-mediated dissociation of NF-kappaB from DNA. *Proc Natl Acad Sci U S A* **111**, 225-230 (2014).
13. H. E. Dembinski *et al.*, Functional importance of stripping in NFkappaB signaling revealed by a stripping-impaired IkappaBalpha mutant. *Proc Natl Acad Sci U S A* **114**, 1916-1921 (2017).
14. D. A. Potoyan, W. Zheng, E. A. Komives, P. G. Wolynes, Molecular stripping in the NF-kappaB/IkappaB/DNA genetic regulatory network. *Proc Natl Acad Sci U S A* **113**, 110-115 (2016).
15. D. A. Potoyan, W. Zheng, D. U. Ferreiro, P. G. Wolynes, E. A. Komives, PEST Control of Molecular Stripping of NFkappaB from DNA Transcription Sites. *J Phys Chem B* **120**, 8532-8538 (2016).
16. B. Berkowitz, D. B. Huang, F. E. Chen-Park, P. B. Sigler, G. Ghosh, The x-ray crystal structure of the NF-kappa B p50.p65 heterodimer bound to the interferon beta -kappa B site. *J Biol Chem* **277**, 24694-24700 (2002).
17. J. W. Chin *et al.*, Addition of p-azido-L-phenylalanine to the genetic code of Escherichia coli. *J Am Chem Soc* **124**, 9026-9027 (2002).
18. J. C. Jewett, C. R. Bertozzi, Cu-free click cycloaddition reactions in chemical biology. *Chem Soc Rev* **39**, 1272-1279 (2010).
19. B. Hua *et al.*, An improved surface passivation method for single-molecule studies. *Nat Methods* **11**, 1233-1236 (2014).

20. B. Hellenkamp *et al.*, Precision and accuracy of single-molecule FRET measurements-a multi-laboratory benchmark study. *Nat Methods* **15**, 669-676 (2018).
21. D. B. Huang *et al.*, Crystal structure of NF-kappaB (p50)2 complexed to a high-affinity RNA aptamer. *Proc Natl Acad Sci U S A* **100**, 9268-9273 (2003).
22. W. Lu *et al.*, OpenAWSEM with Open3SPN2: A fast, flexible, and accessible framework for large-scale coarse-grained biomolecular simulations. *PLoS Comput Biol* **17**, e1008308 (2021).
23. C. S. Sorensen, M. Kjaergaard, Effective concentrations enforced by intrinsically disordered linkers are governed by polymer physics. *Proc Natl Acad Sci U S A* **116**, 23124-23131 (2019).
24. E. Delaforge *et al.*, Investigating the Role of Large-Scale Domain Dynamics in Protein-Protein Interactions. *Front Mol Biosci* **3**, 54 (2016).
25. J. R. Huang *et al.*, Transient electrostatic interactions dominate the conformational equilibrium sampled by multidomain splicing factor U2AF65: a combined NMR and SAXS study. *J Am Chem Soc* **136**, 7068-7076 (2014).
26. A. Callegari *et al.*, Single-molecule dynamics and genome-wide transcriptomics reveal that NF-kB (p65)-DNA binding times can be decoupled from transcriptional activation. *PLoS Genet* **15**, e1007891 (2019).
27. N. C. Lammers *et al.*, Multimodal transcriptional control of pattern formation in embryonic development. *Proc Natl Acad Sci U S A* **117**, 836-847 (2020).
28. S. Bergqvist *et al.*, Kinetic enhancement of NF-kappaBxDNA dissociation by IkappaBalpha. *Proc Natl Acad Sci U S A* **106**, 19328-19333 (2009).
29. C. H. Croy, S. Bergqvist, T. Huxford, G. Ghosh, E. A. Komives, Biophysical characterization of the free IkappaBalpha ankyrin repeat domain in solution. *Protein Sci* **13**, 1767-1777 (2004).
30. J. A. Lamboy, H. Kim, H. Dembinski, T. Ha, E. A. Komives, Single-molecule FRET reveals the native-state dynamics of the IkappaBalpha ankyrin repeat domain. *J Mol Biol* **425**, 2578-2590 (2013).